Possibility of Si-based new material for thin-film solar cell applications

T Suemasu
Institute of Applied Physics, University of Tsukuba, 1-1-1 Tennohdai, Tsukuba, Ibaraki 305-8573, Japan.

E-mail: suemasu@bk.tsukuba.ac.jp

Abstract. We grow $BaSi_2$ epitaxial films on Si(111) substrates by molecular beam epitaxy, and investigate their optical properties such as optical absorption coefficients, minority-carrier diffusion length, and minority-carrier lifetime. These are key parameters which determine the solar cell performance. The band gap of $BaSi_2$ is measured to be approximately 1.3 eV. The absorption coefficient reaches approximately 3×10^4 cm^{-1} at 1.5 eV. The minority-carrier diffusion length and minority-carrier lifetime are found to be about 10 μm and 8 μs, respectively. These values are sufficiently large for thin-film solar cell applications. Internal photoresponse spectra are deduced from data obtained experimentally.

1. Introduction

Recently photovoltaic solar cells have been attracting considerable attention. At present, approximately 90% of solar cells are based on crystalline Si because of its earth-abundance and developed technologies.Thin-film solar cell materials such as CIGS, CZTS, CdTe, and organic materials have been attracting increasing attention due to their high efficiency and low cost. In contrast, the optical absorption layers of crystalline Si solar cells tend to be much thicker than conventional thin-film solar cells, because the optical absorption coefficient α is much smaller for crystalline Si. Therefore, novel Si-based materials for high-efficiency thin-film solar cells have received significant interest. However, little steadfast effort has been devoted to any materials other than Si, CZTS, CIGS, CdTe and III-V compounds as far as inorganic semiconductors are concerned. Among such materials, we have focused much attention on semiconducting $BaSi_2$. The band gap of $BaSi_2$ is approximately 1.3 eV [1,2], and can be increased up to 1.4 eV in $Ba_{1-x}Sr_xSi_2$[3], which matches the ideal solar spectrum much better than crystalline Si. In addition, $BaSi_2$ has a very large absorption coefficient of approximately 3×10^4 cm^{-1} at 1.5 eV [2]. A large value of α and expansion of the band gap in $Ba_{1-x}Sr_xSi_2$ were theoretically expected [4,5]. In solar cells, both absorption coefficient α and minority-carrier diffusion length L are critical. In order to efficiently extract photogenerated carriers, the diffusion length should be larger than the absorption length. Direct band gap semiconductors like GaAs usually have large absorption coefficient. But this generally comes with faster recombination and hence relatively smaller diffusion length. In contrast, both α and L were found to be large enough in $BaSi_2$ (L~10μm) [2,6]. This is because $BaSi_2$ is an indirect band gap semiconductor with a direct transition 0.1 eV above the band edge. Recently, we successfully achieved large photoresponsivity and internal quantum efficiency exceeding 70% in 0.4μm-thick *a*-axis-oriented $BaSi_2$ epitaxial layers [7].

Excess carrier recombination mechanisms in $BaSi_2$ have also been studied [8].These results have spurred interest in this material.

Control of the conductivity of $BaSi_2$ by impurity doping is a requirement because the basic structure of a solar cell is a *p-n* junction. According to Imai and Watanabe [9], substitution of Si in the $BaSi_2$ lattice is more favorable than substitution of Ba from an energetic point of view by first-principles calculation. In our previous works, the electron concentration of Sb-doped n-type $BaSi_2$ was controlled in the range between 10^{16} and 10^{20} cm^{-3} at room temperature (RT) [10]. Very recently, we have achieved the hole concentration exceeding 10^{19} cm^{-3} in B-doped p-type $BaSi_2$. The hole concentration of B-doped $BaSi_2$ was controlled in the range between 10^{16} and 10^{20} cm^{-3} at RT. In this article, the current status and future prospect of this material towards high-efficiency and thin-film solar cell applications are reviewed.

2. Experimental procedures

An ultrahigh vacuum (UHV) chamber equipped with a Knudsen cell for Ba and an electron beam gun for Si was employed. Before the growth, the Si(111) substrates were prepared by subjecting them to the following treatment. The substrates were washed using RCA clean steps, which removed organic and metallic contaminants. The substrates were then annealed at 830 °C for 30 min in the UHV (1×10^{-6} Pa) chamber to remove the protective SiO_2 layers. After annealing, a 7×7 streaky reflection high-energy electron diffraction (RHEED) pattern was observed, indicating a clean Si surface. A two-step growth method was adopted, which included reactive deposition epitaxy (RDE; Ba deposition on hot Si) and molecular beam epitaxy (MBE; co-deposition of Ba and Si) to form thick $BaSi_2$ films [11,12]. The RDE process was carried out for deposition of a template layer as a $BaSi_2$ precursor prior to the subsequent MBE process. The same growth method was successfully utilized for the epitaxial growth of semiconducting β-$FeSi_2$ films on both Si(001) and Si(111) substrates [13,14]. The crystalline quality of the films was evaluated using RHEED and θ-2θ X-ray diffraction (XRD) measurements using Kα x-rays.

3. Results and discussions

3.1. Optical absorption properties

For measurements of optical absorption coefficients, we fabricated the silicon-on-insulator (SOI) substrates using wafer bonding at room temperature (RT) as well as chemical mechanical polishing (CMP). First, 500-μm-thick high-resistive FZ-Si(111) ($\rho > 1000$ Ω·cm) and 500-μm-thick fused silica wafers were bonded at RT. Then, the Si wafer was mechanically ground and polished by CMP down to about 0.7 μm thickness. Prior to loading the substrates into the MBE chamber, oxide layers on the surface of the SOI substrate were etched away by diluted hydrofluoric acid. Thermal treatment was performed at 590 °C for 20 min in UHV to clean the hydrogen-terminated surface. A 20-nm-thick $BaSi_2$ template layer was then formed at 525 °C using RDE, prior to the deposition of an 80-nm-thick $BaSi_2$ layer by MBE (sample A). Si and Ba atoms were co-deposited at 575°C by an electron-beam gun and a Knudsen cell, respectively. For comparison, $BaSi_2$ layers were also epitaxially grown on a Si(111) substrate (sample B) in the same manner as described previously [12]. RHEED and θ-2θ XRD patterns were utilized to evaluate the crystalline quality of the $BaSi_2$ layers. We employed a JASCO U-best 570 spectrophotometer to obtain the transmission spectra of the samples. We observed the (1×1) streaky pattern of Si(111) after thermal cleaning at 590°C.

Figures 1(a) and 1(b) show RHEED patterns of the RDE-grown $BaSi_2$ template layer. The incident electron beam was along the (a) Si[1-10] and (b) Si[11-2] directions. After the RDE growth, we confirmed that the $BaSi_2$ film was epitaxially grown on the Si layer of the SOI substrate as shown in Figs. 1(c) and 1(d). Since these patterns could also be observed at the end of MBE growth, we determined that the $BaSi_2$ film was indeed grown epitaxially.

Figure 2 shows the θ-2θ XRD patterns of samples A and B, $BaSi_2$ films grown on the SOI and Si(111) substrates, respectively. We can see diffraction peaks only from (100)-oriented $BaSi_2$ planes, such as the (200), (400), (600) planes. For the $BaSi_2$ epitaxial film on the SOI substrate, the peak intensities of these planes were almost the same as those in the $BaSi_2$ epitaxial film on the Si(111) substrate. These results indicate that the crystalline quality of the $BaSi_2$ film on the SOI substrate was equivalent to that on the single-crystalline Si(111) substrate.

The transmission spectrum for the $BaSi_2$/SOI structure is presented in Fig. 3. This spectrum was significantly influenced by an interference effect within the 0.7-μm-thick Si layers. The Si layers were very thin and flat due to the CMP process, so that these interference fringes were superimposed on the spectrum. We used the equations presented in Ref. 15 to derive the interference-free transmission spectrum. As shown in Fig. 3, the transmission spectrum was fitted by the maximal extremes of the interference fringes (T_M) and also by their minimal extremes (T_m). Assuming that the Si layers have a certain absorption coefficient on a transparent substrate, the interference-free transmission spectrum T_α can be expressed as just the geometric mean of T_M and T_m ($T_\alpha=\sqrt{T_M\ T_m}$) over the entire region of the transmission spectrum. We calculated the T_α values using the T_M and T_m curves, and also eliminated the absorption due to the Si layers by measuring the transmission spectrum of another SOI substrate. We finally normalized T_α by taking the reflectivity of the sample into consideration. Using T_α, we could obtain the absorption spectrum shown in Fig. 4(a). The absorption coefficient of $BaSi_2$ reached 3×10^4 cm^{-1} at 1.5 eV. Figure 4(b) shows the $(\alpha dh\nu)^{1/2}$ versus hν plot for deriving the indirect optical absorption edge. The straight fit line intersects the horizontal axis at 1.34 eV. Thus, the indirect absorption edge with phonon emission was 1.34 eV. The absorption with phonon absorption is neglected, because the fitting was performed at the higher-energy region than the indirect band gap. Thus, the indirect band gap is determined to be approximately 1.32 eV, assuming that the phonon energy is approximately 25 meV. It is true that absorption coefficients below 10^2 cm^{-1} are necessary to determine the precise energy gap. Much thicker $BaSi_2$ enables us to measure smaller absorption coefficients free from errors. In addition, we can't rule out the possibility that defects contribute to absorption to some extent in the energy range below 1.34 eV.

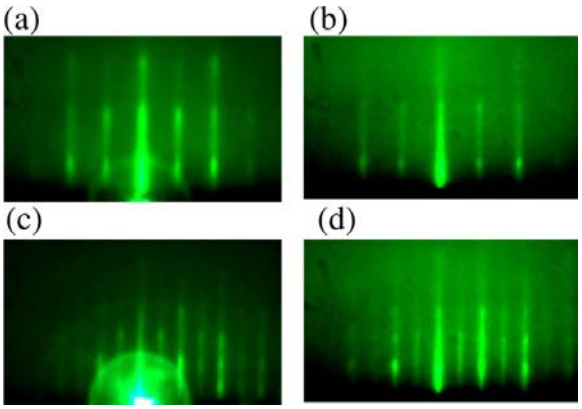

Figure 1. RHEED patterns of $BaSi_2$ in sample A, observed after (a)(b) RDE and (c)(d)MBE growth along the (a)(c) Si[1-10] and (b)(d) Si[11-2] azimuths.

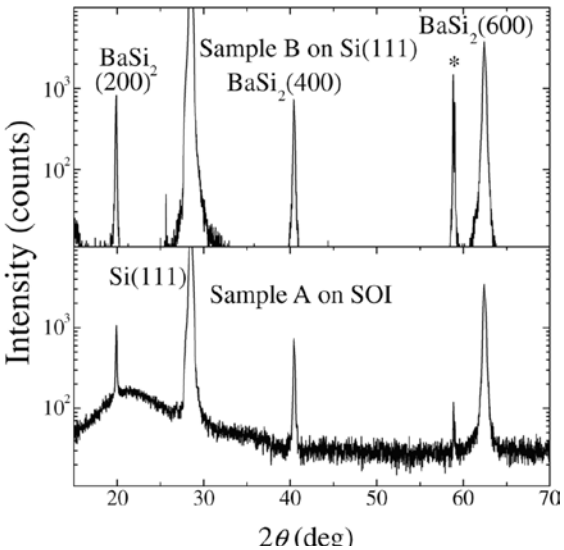

Figure 2. *θ-2θ* XRD patterns for samples A and B, grown on SOI and Si(111) substrates, respectively. The forbidden diffraction peak of Si(222) indicated by asterisk occurs by double diffraction.

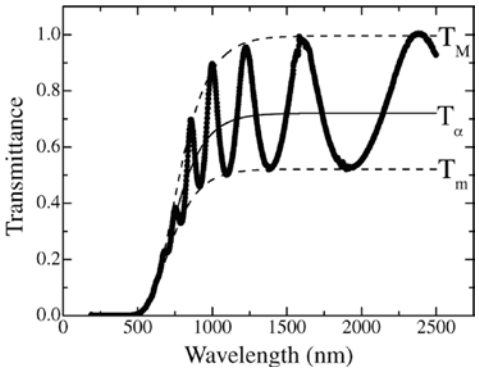

Figure 3. Transmission spectrum for sample A, where $T_\alpha = \sqrt{T_M T_m}$.

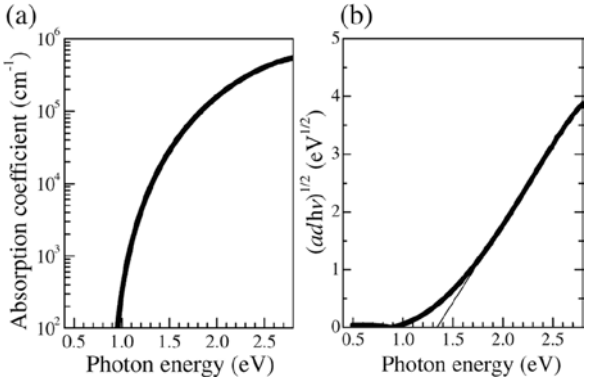

Figure 4. (a) Absorption spectrum for sample A. (b) $(\alpha d h\nu)^{1/2}$ versus $h\nu$ plot for sample A.

3.2. Minority-carrier properties

3.2.1. Minority-carrier diffusion length

For measurements of minority-carrier diffusion length in undoped $BaSi_2$, we fabricated 300-nm-thick undoped n-$BaSi_2$ films by RDE at 550 °C for 5 min, followed by MBE at 600 °C for 120 min. Undoped $BaSi_2$ shows n-type conductivity with electron concentrations of approximately 10^{16} cm^{-3} [1]. In order to investigate the grain size of $BaSi_2$ and grain boundaries (GBs), plan-view transmission electron microscopy (TEM) samples prepared by mechanical polishing and ion milling were observed using TOPCON EM-002B operated at 120 kV. For electron beam induced current (EBIC) measurements, Al/n-$BaSi_2$ Schottky diodes were formed. Front-side Schottky contacts were formed with Al on the $BaSi_2$ surface via wire bonding, and the back-side ohmic contact was made with Al by sputtering. EBIC observations were carried out in the edge-scan configuration with a Hitachi S4300 field-emission scanning electron microscope (SEM) in the EBIC mode at RT. The acceleration voltage of the electron beam, V_{ac}, was set at 5 kV to avoid penetration of the beam into the Si substrate. The penetration depth of the electron beam is estimated to be shorter than 300 nm, which is the thickness of the $BaSi_2$ layers, when V_{ac} is 5 kV, with the density of $BaSi_2$ being 5.14 g/cm^3.

Figures 5(a)(b) and 5(c)(d) show secondary-electron (SE) and EBIC images around the Al contact, respectively, with V_{ac} = 5 kV. In the EBIC method, carriers generated within the diffusion length in the n-type $BaSi_2$ are collected by the electric field under the Al contact and sensed as a current in the external circuit. In Figs. 5(c)(d), the brighter regions show higher collection of electron-beam-induced carriers in the $BaSi_2$. We cannot see defect-related black lines. Figure 6 shows the EBIC line-scan data along dotted line AA' in Fig. 5(c). The EBIC profile shows an exponential dependence of the distance from the Al contact. In this work, the diffusion length of minority carriers was roughly estimated to be approximately 10 μm, assuming that the EBIC profile varies as exp(-x/L), where x is the distance from the Al edge (point A) along the dotted line, and L is the diffusion length of holes for $BaSi_2$. The obtained minority-carrier diffusion length is much larger than the grain size of the $BaSi_2$, implying that the GBs do not work as defect centers for minority carriers in n-$BaSi_2$. The contribution of carriers generated within the n-Si substrate to the measured EBIC signals can be excluded, because the simulated penetration depth of the electron beam is shorter than 300 nm, the thickness of the $BaSi_2$ layers, when V_{ac} is 5 kV. Thus, it is reasonable to think that the number of carriers generated within the Si substrate was negligibly small compared to those generated in the $BaSi_2$ layers. To confirm the GBs character, an EBIC system with spatial resolutions less than 0.1 μm may be necessary. We should also

note here that the obtained minority-carrier diffusion length is roughly 30 times larger than $1/\alpha$ (=0.3 μm) at 1.5 eV, suggesting that this value is large enough for solar cell applications.

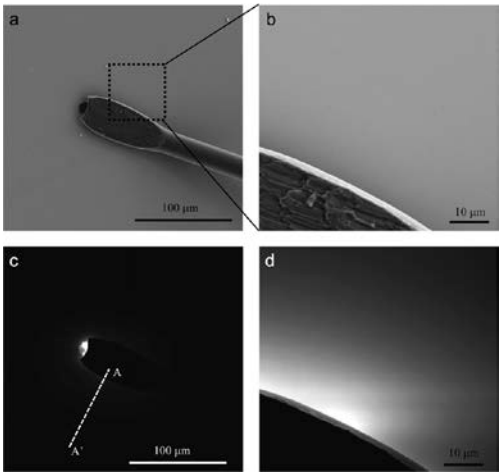

Figure 5. (a)(b) SE and (b)(d) EBIC images around the Al contact.

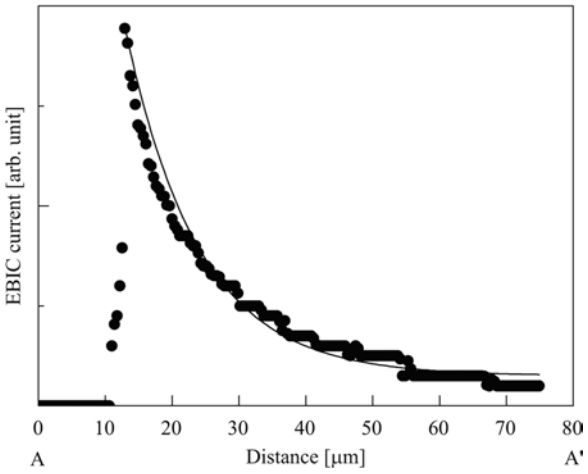

Figure 6. Experimental and simulated (solid line) EBIC line-scan profiles along the dotted line from points A to A' in Fig. 5(c).

3.2.2. Minority-carrier lifetime diffusion length

After cleaning a floating-zone n-Si(111) substrate (ρ>1000 Ω·cm) at 900 °C for 30 min in UHV, a 5-nm-thick $BaSi_2$ template layer was grown on the Si substrate by RDE, followed by MBE to form a 1.5-μm-thick $BaSi_2$ epitaxial film. Figure 7 shows the relationship between apparent minority-carrier life time τ_a and excess-carrier density of the 1.5-μm-thick $BaSi_2$. The undoped $BaSi_2$ shows n-type conductivity and the electron concentration is about 10^{16} cm^{-3} [1]. The excess carrier concentration was calculated from the absorption coefficient of $BaSi_2$ at 349 nm, and the irradiated laser intensity, which was varied from 1.1×10^2 to 1.3×10^2 W/cm^2. The inset shows the decay curve when the excess carrier concentration was 7.4×10^{16} cm^{-3}. Decay can be divided into two modes in terms of decay rate. We see initial rapid decay, followed by approximately constant decay. According to our previous work, the rapid decay is caused by Auger recombination [8]. τ_a was calculated by approximating the tail region of the decay curve by a single exponential curve. We see that τ_a decreases with increasing the excess-carrier density. This is because the excess-carrier density is several orders of magnitudes higher than majority-carrier density at equilibrium in undoped n-$BaSi_2$. Such high carrier injection leads to multicarrier recombination. Therefore, when we discuss about the minority-carrier lifetime, we should use lower injection value. As can be seen in Fig. 7, τ_a becomes independent of excess-carrier density when the excess carrier concentration becomes smaller than 10^{16} cm^{-3}, indicating that τ_a corresponds to the effective minority-carrier lifetime τ in this region. This result makes sense because the electron concentration of undoped n-$BaSi_2$ is about 10^{16} cm^{-3} [1]. Therefore, it

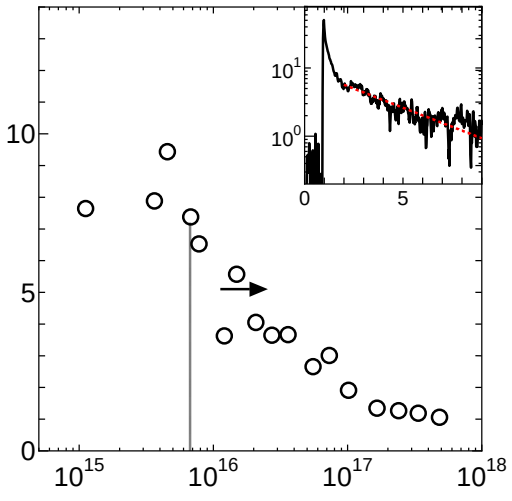

Figure 7. Relationship between minority-carrier life time and excess-carrier density of 1.5-μm-thick $BaSi_2$. The inset shows the photoconductivity decay curve of the 1.5-μm-thick $BaSi_2$ film when the excess-carrier concentration is 7.4×10^{16} cm^{-3}.

is reasonable to think that the minority-carrier lifetime in the 1.5-μm-thick $BaSi_2$ is about 8 μs. Assuming that the hole mobility is 1 $cm^2V^{-1}s^{-1}$ [16], the minority-carrier diffusion length L is estimated to be about 4.5 μm from the equation of $L = \sqrt{k_B T \mu \tau / q}$. Here, k_B is the Boltzmann constant, T the absolute temperature, μ the mobility of holes, τ the effective minority-carrier lifetime, and q the elemental charge. This value is about three times larger than the absorption layer thickness (~1.5 μm) in a $BaSi_2$ pn junction diode. On the basis of these results, we achieved the formation of high-quality $BaSi_2$ films thicker than 1.5 μm, where the minority-carrier lifetime was large enough for thin-film solar cell applications.

3.3. Expected spectral response in a $BaSi_2$ pn junction diode

We attempted to deduce the expected photocurrent density in a $BaSi_2$ p^+n homojunction diode. Analytical expressions for the photogenerated and dark saturation current densities can be obtained only when the dopant concentration, carrier lifetime and other parameters are assumed constant. Suppose here a simple p^+n abrupt junction diode in samples pn-A to pn-E as shown in Table 1. N_A, W_e, L_e, S_e are the acceptor density, neutral p^+ layer width, minority-carrier (electrons) diffusion length, and surface recombination velocity, and N_D, W_b, L_h, and S_h are their counterparts in the n layer. W is the depletion region width.

Table 1. Parameters of $BaSi_2$ homojunction diode are shown.

Sample	N_A (cm^{-3})	W_e (μm)	L_e (μm)	S_e (cm/s)	W (μm)	N_D (cm^{-3})	W_b (μm)	L_h (μm)	S_h (cm/s)
pn-A	10^{18}	0.1	0.1	8	0.4	10^{16}	1.5	10	8
pn-B	10^{18}	0.1	0.1	8	0.4	10^{16}	2.5	10	8
pn-C	10^{18}	0.05	0.1	8	0.4	10^{16}	1.5	10	8
pn-D	10^{18}	0.05	0.1	100	0.4	10^{16}	1.5	10	8
pn-E	10^{18}	0.05	0.1	8	0.4	10^{16}	1.5	10	100

The total photocurrent density j at energy E per unit energy is given by the sum of current due to electrons generated within the neutral p^+-$BaSi_2$ region, j_e, current due to electron-hole pairs generated within the depletion region, j_{DL}, and current due to holes generated within the neutral n-$BaSi_2$ region, j_h. The internal quantum efficiency, *IQE*, is equal to,

$$IQE(E) = \frac{j}{q\Phi_0(1-R)} = \frac{j_e + j_{DL} + j_h}{q\Phi_0(1-R)} \qquad (1)$$

Once the *IQE* is derived, the J_L is given by,

$$J_L = q\int \Phi_0(1-R)\, IQE(E)\, dE \qquad (2)$$

In order to make J_L large, we should minimize R and maximize *IQE* over the solar spectral range. Therefore, the *IQE* is a measure of the quality of the diode. The contribution to the *IQE* by j_{DL}, j_e and j_h, that is IQE_{DL}, IQE_e, and IQE_h, respectively, are obtained analytically. Then, we investigated the dependence of *IQE* on various parameters. Regarding the α, we used the experimental data shown in ref 1. While the diffusivity is not highly sensitive to impurity and defect, we thus set both D_e and D_h to be 0.1 cm^2/s, because L_h is 10 μm and τ_h is 10 μs as described earlier. When the impurity concentrations in the p^+ and n layers, that is N_A and N_V, are set to be 10^{18} and 10^{16} cm^{-3}, respectively. In this case, the W is estimated to be 0.4 μm and the built-in voltage 1.0 V assuming that the permittivity of $BaSi_2$ is approximately 15, and the effective densities of states of the conduction band

and valence band, that is, N_C and N_V, respectively, are 2.6×10^{19} and 2.0×10^{19} cm^{-3}.[4] The square of the intrinsic carrier concentration, n_i, at RT is calculated to be $n_i^2 = 8\times10^{16}$ cm^{-3}. Other parameters are summarized in Table 1. In Figs. 8(a) and 1(b), the *IQE* is almost the same between samples pn-A and pn-B although the W_b is increased from 1.5 μm in sample pn-A to 2.5 μm in sample pn-B, meaning that W_b=1.5 μm is enough. We see that when the W_e is decreased from 0.1 to 0.05 μm, the *IQE* is increased particularly in higher energies in samples pn-C to pn-E. This is attributed to the enhancement of IQE_e and IQE_{DL}. Since the absorption coefficient of $BaSi_2$ is large, the contributions of the surface p^+-layer and the depletion region to the *IQE* becomes pronounced when the W_e is decreased. This result implies that we design the W_b to be equal to L_e or smaller. In samples pn-C to pn-E, there is no significant difference in *IQE* regardless of different S_e and S_h. This means that the *IQE* is not so sensitive to surface conditions in a $BaSi_2$ homojunction solar cell. We next discuss the expected conversion efficiency of the diodes. Considering that n_{p0} is much smaller than p_{n0} because of the p^+n junction, the dark current density of the diode, J_{dark}, is dominant from the contribution of n-type layer, and thus, the reverse saturation current density J_s is obtain. The J_s and J_L values, and the expected open-circuit voltage, V_{OC}, under AM1.5 illumination for samples pn-A to pn-E are investigated, assuming that the fill-factor, *FF*, is 0.8 regardless of V_{OC} and R=0. As a result, the conversion efficiency is calculated to be more than 25% in samples pn-C and pn-D even though the total layer thickness is only 2 μm.

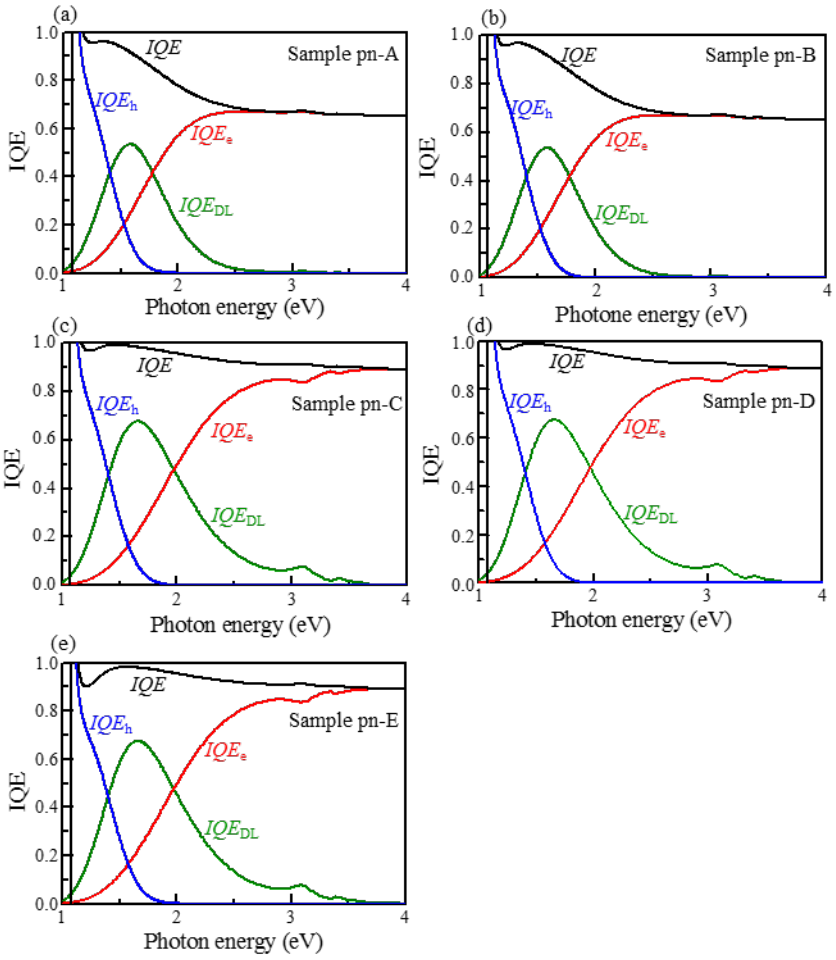

Figure 8. Calculated internal spectral responses for samples pn-A to pn-E. Individual contributions of IQE_e, IQE_{DL}, and IQE_h to *IQE* are shown.

4. Summary

Current status toward Si-based high-efficiency thin-film solar cells was reviewed in terms of optical absorption properties and minority-carrier properties. These are key parameters which determine the performance of solar cells. The band gap of $BaSi_2$ was measured to be approximately 1.3 eV. The absorption coefficient reached approximately 3×10^4 cm^{-1} at 1.5 eV. The minority-carrier diffusion length and minority-carrier lifetime were found to be about 10 μm and 8 μs, respectively. In particular, what's interesting with $BaSi_2$ is that it has large absorption coefficients and at the same time large minority-carrier diffusion length. This feature, caused by the fact that the direct transition starts just 0.1 eV above the band edge, is favourable to effectively extract photogenerated carriers. We calculated the photoresponse spectra of $BaSi_2$ p^+n homojunction diodes using experimentally obtained absorption coefficients and minority-carrier diffusion length, and discussed the influence of parameters such as emitter and base layer thicknesses, surface recombination velocities. The *IQE* is not so sensitive to S_e and S_h, and W_b, while the W_e has a significant influence on *IQE* particularly in a high energy region. This is because the absorption coefficient of $BaSi_2$ is large. Thus, we need to take care of the relationship between W_e and L_e in the emitter layer when we design the W_e. The conversion efficiency exceeding 25% is expected for 2 μm-thick $BaSi_2$ homojunction diodes in an ideal condition.

[1] Morita K, Inomata Y and Suemasu T 2006 *Thin Solid Films* **508** 363
[2] Toh K, Saito T and Suemasu T 2011 *Jpn. J. Appl. Phys.* **50** 068001
[3] Morita K, Kobayashi M and Suemasu T 2006 *Jpn. J. Appl. Phy*. **45** L390
[4] Migas D B, Shaposhnikov V L and Borisenko V E 2007 *Phys. Status Solidi* B **244** 2611
[5] Imai Y and Watanabe A 2007 *Thin Solid Films* **515** 8219
[6] Baba M, Toh K, Toko K, Saito N, Yoshizawa N, Jiptner K, Sekiguchi T, Hara K O, Usami N and Suemasu T 2012 *J. Cryst. Growth* **348** 75
[7] Du W, Suzuno M, Khan M. A, Toh K, Baba M, Nakamura K, Toko K, Usami N and Suemasu T 2012 *Appl. Phys. Lett.* **100** 152114
[8] Hara K O, Usami N, Toh K, Baba M, Toko K and Suemasu T 2012 *J. Appl. Phys*. **112** 083108
[9] Imai Y and Watanabe A 2007 *Intermetallics* **15** 1291
[10] Kobayashi M, Matsumoto Y, Ichikawa Y, Tsukada D, and Suemasu T 2008 Appl. Phys. Express **1** 05403
[11] Inomata Y, Nakamura T, Suemasu T and Hasegawa F 2004 *Jpn. J. Appl. Phys.* **43** 4155
[12] Inomata Y, Nakamura T, Suemasu T and Hasegawa F 2004 *Jpn. J. Appl. Phys*. **43** L478
[13] Tanaka M, Kumagai Y, Suemasu T and Hasegawa F 1997 *Jpn. J. Appl. Phys*. **36** 3620
[14] Hiroi N, Suemasu T, Takakura K, Seki N and Hasegawa F 2001 *Jpn. J. Appl. Phys.* **40** L1008
[15] Swanepoel R 1983 *J. Phys.* E **16** 1214
[16] Khan M A, Hara K O, Du W, Baba M, Nakamura K, Suzuno M, Toko K, Usami N and Suemasu T 2013 *Appl. Phys. Lett.* **102** 112107